Available online at www.sciencedirect.com
SCIENCE DIRECT
Journal of Power Sources 157 (2006) 302–310
JOURNAL OF POWER SOURCES
www.elsevier.com/locate/jpowsour

Radiation heat transfer in planar SOFC electrolytes

K.J. Daun*, S.B. Beale, F. Liu, G.J. Smallwood

National Research Council of Canada, Institute for Chemical Process and Environmental Technology, Ottawa, Ont., Canada K1A 0R6

Received 7 July 2005; accepted 18 July 2005
Available online 31 August 2005

Abstract

Because of their high operating temperatures, there has been speculation that thermal radiation may play an important role in the overall heat transfer within the electrode and electrolyte layers of solid oxide fuel cells (SOFCs). This paper presents a detailed characterization of the thermophysical and radiative properties of the composite materials, which are then used to define a simple 2D model incorporating the heat transfer characteristics of the electrode and electrolyte layers of a typical planar SOFC. Subsequently, the importance of thermal radiation is assessed by comparing the temperature field obtained using a conduction model with those obtained using two coupled conduction/radiation models. Contrary to some published literature, these results show that radiation heat transfer has a negligible effect on the temperature field within these components, and does not need to be accommodated in comprehensive thermal models of planar SOFCs.

Keywords: SOFC; Thermal radiation; Electrolyte

1. Introduction

Due to their high thermal efficiency, high quality of heat output, and fuel flexibility, solid oxide fuel cells (SOFCs) may soon replace more traditional devices currently used to generate electricity in many applications. Thermal modeling is integral part to the development of this emerging technology, since the temperature field is needed to calculate the electrochemical reaction rates, electrode overpotentials, and Ohmic resistances that govern fuel cell performance. Furthermore, an accurate thermal analysis is required to assess the mechanical soundness of the device, as typical SOFC operating temperatures approach the service temperatures of the component materials.

Because of their high operating temperatures (typically 800–1200 K), there has been some speculation that thermal radiation may be an important component of heat transfer within SOFCs. Several studies have focused on the effect of radiation heat transfer in the fuel and air channels within planar and tubular SOFCs [1–3]. These studies have all found that this phenomenon plays a minor effect on the overall temperature distribution within the fuel cell relative to other modes of heat transfer.

The present work instead focuses on radiation heat transfer within the solid anode, electrolyte, and cathode SOFC layers. Although it may seem unlikely that radiation could be important within these solid ceramic and cermet layers, this is in fact not an unreasonable hypothesis given the high temperatures involved and the thickness of the electrode and electrolyte layers. Indeed, thermal radiation is known to be an important mode of heat transfer through ceramic thermal barrier coatings used in high temperature applications, which have approximately the same thickness as the ceramic electrolyte layer in the present application [4].

Nevertheless, detailed study of radiation transfer through the SOFC electrode and electrolyte layers has been quite limited to date. Murthy and Fedorov [5] analyzed radiation heat transfer between the air and fuel channels in a two-dimensional electrolyte-supported counter-flow SOFC. Radiation heat transfer through the optically-thin electrolyte was modeled using the Schuster–Schwarzchild two-flux method, while radiation within the optically-thick electrodes was simulated by the diffusion approximation. Both radiation models

* Corresponding author. Tel.: +1 613 993 1289; fax: +1 613 941 1571.
E-mail address: kyle.daun@nrc-cnrc.gc.ca (K.J. Daun).

0378-7753/$ – see front matter.
doi:10.1016/j.jpowsour.2005.07.045

Nomenclature

c_p	specific heat ($J\,kg^{-1}\,K^{-1}$)
$E_b(\lambda)$	blackbody emissive power ($W\,m^{-2}$)
F	Faraday's constant, $96.487 \times 10^3\ V\,mol^{-1}$ electrons^{-1}
h	convection coefficient ($W\,m^{-2}\,K$)
i''	current density ($A\,m^{-2}$)
k	thermal conductivity ($W\,m^{-1}\,K^{-1}$)
$\dot{m}'$	mass flow rate per unit channel thickness ($kg\,s^{-1}\,m$)
M	molar mass ($kg\,mol^{-1}$)
Nu_{D_h}	Nusselt number
q''	heat flux ($W\,m^{-2}$)
q'''	volumetric heat source ($W\,m^{-3}$)
S	molar entropy ($J\,mol^{-1}\,K^{-1}$)
t_a	anode layer thickness (μm)
t_c	cathode layer thickness (μm)
t_e	electrolyte layer thickness (μm)
T	temperature (K)
u	utilization rate
y	mole fraction

Greek letters

α	absorption coefficient (m^{-1})
δ	reaction zone thickness (μm)
ε	surface emissivity
η	electrode overpotential (V)
λ	wavelength (μm)
ρ	density ($kg\,m^{-3}$)
ρ_e	electrolyte ohmic resistivity (Ω m)
σ_s	scattering coefficient (m^{-1})
Ω	scattering albedo, $\sigma_s/(\alpha+\sigma_s)$

Subscripts

a	anode
c	cathode
e	electrolyte
rev	reversible
irr	irreversible

were incorporated into a coupled CFD/electrochemistry simulation of the temperature field. This study found that ignoring radiation heat transfer caused errors of more than 10% (approximately 100 K) in the temperature field.

More recently, Damm and Fedorov [6] studied radiation within a two-dimensional anode-supported counter-flow SOFC. The Schuster–Schwarzchild method was again used to model radiation heat transfer through the electrolyte, but in this treatment the electrodes were both assumed to be opaque and consequently excluded from the radiation analysis. In contrast to the previous paper, this study found that neglecting radiation in the thermal model accounts for only a few degrees error in the SOFC temperature field. The authors attribute the difference between their results and those of Murthy and Fedorov [5] to the different SOFC geometries studied.

In this paper we seek to determine if radiation heat transfer is an important phenomenon in the electrode and electrolyte layers of typical planar SOFCs. This is done by first performing a detailed analysis of the thermophysical and optical properties of the component materials. Next, a simplified 2D thermal model of an anode-supported SOFC is developed, based on the important heat transfer and heat generation mechanisms in the fuel cell. Finally, the importance of thermal radiation relative to other modes of heat transfer is assessed by comparing the temperature field within the electrode and electrolyte layers obtained using a conduction model to those obtained using coupled conduction/Monte Carlo and conduction/Schuster–Schwarzchild models. These results show that thermal radiation has only a minimal effect on the temperature field, suggesting that this phenomenon can be excluded from detailed SOFC thermal models.

2. Heat transfer in solid oxide fuel cells

2.1. Solid oxide fuel cells

Solid oxide fuel cells are solid state devices that convert the chemical potential in fuel and oxygen directly into electricity by taking advantage of the capacity of zirconia to conduct oxygen ions. A cell consists of three layers, as shown in Fig. 1: an anode layer typically composed of porous cermet (most often a combination of Ni and yittria-stabilized zirconia, YSZ), a solid electrolyte layer composed of YSZ, and a cathode usually made up of porous strontium-doped lanthanum magnate ($LaMnO_3$), a perovskite. These layers are arranged in planar or tubular configurations to create a single cell (this paper focuses on the planar arrangement.) One of the three layers provides structural support and is consequently thicker than the other two; the majority of SOFCs are anode- or cathode-supported, since a thin electrolyte layer

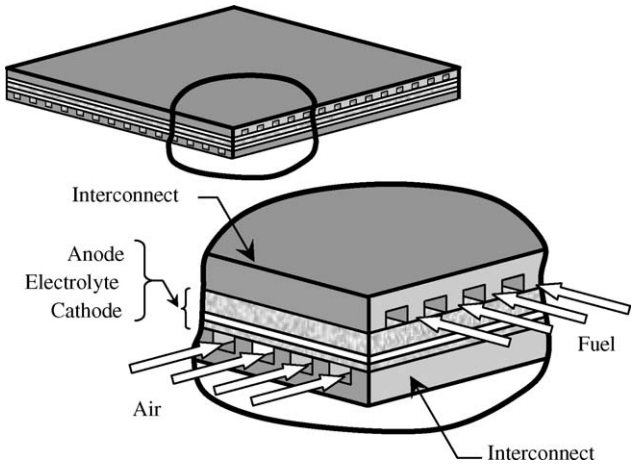

Fig. 1. Solid oxide fuel cell.

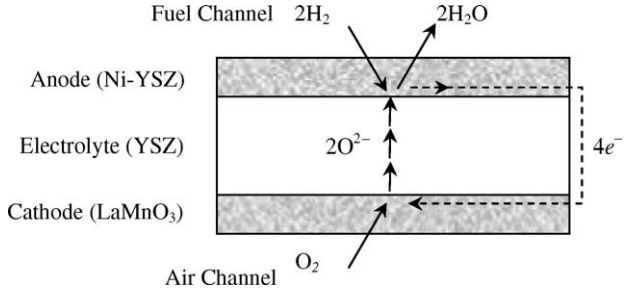

Fig. 2. Schematic of electrochemical reactions.

facilitates ion transfer between the electrodes. Air channels provide oxygen to the cathode, while fuel channels provide hydrogen and remove water vapor from the anode. Individual SOFC cells are encased in a stainless-steel or ceramic interconnect and then connected electrically to form a stack.

Electricity is generated by the electrochemical reactions at the electrode–electrolyte interfaces, as shown in Fig. 2. (The porosity of the electrodes enables the reactants and products to migrate between the electrode surface and the electrode–electrolyte interface.) At the cathode–electrolyte interface, oxygen is combined with electrons supplied by the interconnect to yield oxygen ions

$$O_2 + 4e^- \rightarrow 2O^{2-}. \quad (1)$$

The oxygen ions travel across the electrode to the anode–electrolyte interface. Here, they combine with the hydrogen fuel to yield water and electrons

$$2O^{2-} + 2H_2 \rightarrow 2H_2O + 4e^-, \quad (2)$$

which are removed by the fuel channel and interconnect respectively. Thus, the overall chemical reaction is

$$2H_2 + O_2 \rightarrow 2H_2O. \quad (3)$$

If CH_4 is used as a fuel, additional reforming reactions occur within the fuel channel and at the anode surface; in this work, the only fuel considered is H_2. A thorough description of the structure and electrochemistry within a solid oxide fuel cell is provided by Beale [7].

2.2. Heat transfer mechanisms

Heat is generated by reversible and irreversible mechanisms inside the electrode and electrolyte layers, and is removed predominantly by convection through the air and fuel channels.

In the majority of SOFC simulations, the overall heat generation rate is first calculated by applying the first law of thermodynamics to Eq. (3), subsequently modeled as either uniform volumetric generation through the electrolyte [2], or a uniform planar heat source at the cathode/electrolyte interface [8]. Although this treatment is sufficient to provide a rough approximation of the large-scale temperature variation within a SOFC, a more accurate estimate of the temperature field is required to assess the importance of radiation heat transfer across the electrode and electrolyte layers. Accordingly, in this application each heat generation mechanism is modeled at the location it occurs within the SOFC as described by Khaleel and Selman [9].

Most of the heat generated within the SOFC is due to reversible and irreversible processes occurring at the electrode/electrolyte interfaces within the triple-phase boundaries; since these processes are surface phenomena, the corresponding heat generation terms are appropriately modeled as planar heat sources. Reversible heat generation is due to entropy transfer by the electrochemical reactions at the cathode and anode

$$q''_{\mathrm{rev,c}} = T(2S_{O^{2-}} - S_{O_2} - 4S_{e^-})\frac{i''}{4F} \quad (4)$$

and

$$q''_{\mathrm{rev,a}} = T(2S_{H_2O} - 2S_{H_2} - 2S_{O^{2-}} + 4S_{e^-})\frac{i''}{4F}, \quad (5)$$

where i'' is the local current density, F the Faraday's constant, and the S_x terms denote the molar entropies of the products and reactants at the operating temperature and pressure. Under standard operating conditions entropy is consumed at the cathode and produced at the anode, so Eqs. (1) and (2) are exothermic and slightly endothermic, respectively [9,10]. Eqs. (4) and (5) cannot be solved directly since the molar entropies of half-reaction stages are generally unknown. Instead, an experimentally-determined value for the entropy change at the cathode is taken from Kanamura et al. [10] and the entropy change at the anode is then inferred from the relation $\Delta S_a = \Delta S_{tot} - \Delta S_c$, where ΔS_{tot} is the overall entropy change associated with Eq. (3). (The overall entropy change is calculated assuming all products and reactants are at 1000 K, and partial pressures of O_2, H_2, and H_2O equal to 0.21, 0.75, and 0.25 atm, respectively, which are typical of SOFC operating conditions.)

Irreversible heat generation at the electrode/electrolyte interfaces is caused by the irreversibilities associated with ion transfer across these interfaces that are often referred to as the *cathodic* and *anodic overpotentials*, η_c and η_a, respectively. These quantities are most often expressed in units of volts, and accordingly the corresponding heat generation rates associated with these irreversibilities are $q''_{\mathrm{irr,c}} = i''\eta_c$ and $q''_{\mathrm{irr,a}} = i''\eta_a$.

Although the electrode overpotentials can be estimated from phenomenological equations [7], the present simulation assumes typical values for η_c and η_a based on experimental studies [11,12].

A third source of heat generation is due to volumetric Ohmic heating in the electrolyte due to the conduction of oxygen ions, $q'''_{\mathrm{ohm}} = \rho_e i''^2$, where ρ_e is the ionic resistivity of the electrolyte. (A temperature-dependent correlation of ρ_e is provided in [13].) Although this effect is neglected when simulating most other types of fuel cells, Ohmic heating must be included in SOFC models due to the large ionic resistance

Table 1
Thermal conductivity of SOFC layers

Material	Porosity (%)	k (W m^{-1} K^{-1})
YSZ (electrolyte)	6	2.3 [14]
$LaMnO_3$ (cathode)	40	0.8 [15]
50% Ni-YSZ (anode)	40	3.7 [16]

of YSZ compared to that of electrolyte materials used in other fuel cells.

Heat generated within the electrode and electrolyte layers of the SOFC is removed predominantly by the fuel and air channels. The inlet temperatures of the air and fuel channels determine the lower operating temperature of the fuel cell; in SOFCs, the air and fuel are preheated to approximately 950 K to facilitate electrochemical and reforming reactions that occur within the fuel cell. The upper operating temperature depends on the fuel and air mass flow rates and the rate of energy generation within the fuel cell.

3. Property characterization

As previously mentioned, there is considerable motivation for developing accurate SOFC thermal models, and to that end high-temperature experimental studies have been performed to characterize the thermal conductivities of different SOFC materials [14–16], which are summarized in Table 1.

Far less emphasis has been placed on the experimental determination of radiative properties, since most previous SOFC thermal models have neglected thermal radiation within the composite layers. The electrolyte material is the best characterized of the layers; experimental determination of the radiative properties of polycrystalline YSZ has been largely motivated by its use as a thermal barrier coating. Makino et al. [17] inferred the spectral absorption and scattering properties of 6% porous YSZ by applying a four-flux model to spectral reflection and transmission data obtained from a thin ceramic laminate; these distributions are shown in Fig. 3, along with the shape of Planck's distribution at

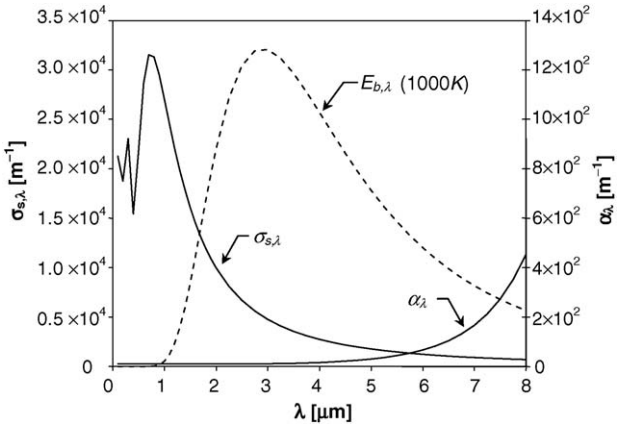

Fig. 3. Radiative properties of YSZ electrolyte [17].

1000 K. Scattering dominates the extinction coefficient at short wavelengths ($\lambda \leq 5\,\mu m$) and is caused by refraction as radiation traverses the solid-pore interface, since the refractive indices of the ceramic and the pore void are different; a rigorous description of this phenomenon is provided by Van de Hulst [18]. (Scattering also occurs at grain boundaries, but to a lesser extent.) Due to the high density of scattering sites within ceramics, radiation is multiply scattered, so the scattering can be assumed to be isotropic [17]. Infrared absorption in YSZ is due to lattice vibrations at long wavelengths ($\lambda > 3\,\mu m$), and can be accurately modeled using Lorentz theory [19]. The Planck mean absorption and scattering coefficients at 1000 K are $\alpha_P = 260\,m^{-1}$ and $\sigma_{sP} = 1 \times 10^4\,m^{-1}$, respectively; these values are used in the heat transfer model presented later in the paper.

Determining the radiative properties of the electrodes is more problematic. A recent study was unable to find the absorption and scattering coefficients of these materials through infrared spectrometry due to their high opacities [6]. Furthermore, numerical modeling of scattering in microporous materials is generally not possible since it is strongly dependent; scattering in the cermet is also complicated by reflection at metal/ceramic interfaces. Despite these difficulties, however, the importance of thermal radiation within the anode and cathode can be assessed by examining the magnitude of the extinction coefficients, which are greater than or equal to the absorption coefficients. These, in turn, are estimated by applying appropriate analytical models to the electromagnetic properties of the bulk materials.

The absorption coefficient of $LaMnO_3$ is estimated by performing a Kramers–Kronig analysis [20] on the spectral, normal reflectance data of a single $LaMnO_3$ crystal presented by Okimoto et al. [21]. This analysis is based on the relationship

$$\delta(\eta) = \frac{\eta}{\pi} \mathrm{PV} \left[\int_0^\infty \frac{\ln \rho_n(\eta')}{\eta^2 - \eta'^2}\, d\eta' \right], \tag{6}$$

where η is the wavenumber, $\rho_n(\eta')$ is the normal reflectivity, PV denotes the Cauchy principle value, and $\delta(\eta)$ is the phase angle of the complex refraction coefficient, defined implicitly as

$$\sqrt{\rho_n(\eta)}[\cos\delta(\eta) + i \sin\delta(\eta)] = \frac{n - ik - 1}{n - ik + 1}. \tag{7}$$

Once Eq. (7) is solved for n and k, the absorption coefficient is found from $\alpha(\lambda) = 4\pi k/n\lambda$, which is plotted in Fig. 4.

The absorption coefficient of the Ni-YSZ anode material is estimated using an effective medium theory [22]. In this approach, the composite is modeled as a homogeneous effective medium having optical properties calculated from those of the constituent materials. The functional relationship used to calculate the optical properties of the effective medium is derived by applying Mie scattering theory to analyze a system consisting of a random unit cell embedded within the effective medium. The random unit cell is made up of the constituent materials in a simplified (usually spherical)

arrangement that represents the composite microstructure, and the optical properties of the effective medium must then make this random unit cell "invisible" when viewed from outside the system. The accuracy and applicability of an effective medium theory as a model for a particular material depends on the microstructure and optical properties of the constituent materials, and consequently the random unit cell used in the derivation of the effective medium theory. Bruggeman's theory is the most suitable for modeling the Ni-YSZ cermet, since the Bruggeman random unit cell assumes that the composite materials enter on an equal footing to form a space-filling random mixture, which describes the microstructure of an anode made by sintering a roughly equal mixture of the constituent materials in powdered form. The complex dielectric function of Bruggeman's effective medium, $\boldsymbol{\varepsilon}_{\mathrm{Br}}$, is found by solving

$$f_{\mathrm{A}}\frac{\boldsymbol{\varepsilon}_{\mathrm{A}}-\boldsymbol{\varepsilon}_{\mathrm{Br}}}{\boldsymbol{\varepsilon}_{\mathrm{A}}+2\boldsymbol{\varepsilon}_{\mathrm{Br}}}+(1-f_{\mathrm{A}})\frac{\boldsymbol{\varepsilon}_{\mathrm{B}}-\boldsymbol{\varepsilon}_{\mathrm{Br}}}{\boldsymbol{\varepsilon}_{\mathrm{A}}+2\boldsymbol{\varepsilon}_{\mathrm{Br}}}=0, \tag{8}$$

where $\boldsymbol{\varepsilon}_{\mathrm{A}}$ and $\boldsymbol{\varepsilon}_{\mathrm{B}}$ are the complex dielectric functions of ZrO_2 [19] and Ni [23], respectively, and f_{A} is the filling factor of the ZrO_2, which is assumed to be 50%. The absorption coefficient of the effective medium is then calculated from $\varepsilon_{\mathrm{Br}}$, and is plotted in Fig. 4.

Fig. 4 shows that the magnitude of the absorption coefficient is such that the mean penetration distance of radiation is not greater than 2 μm and 2 nm for the cathode and anode materials, respectively. The actual mean penetration distances are less than these estimates since scattering has been neglected in the extinction coefficient and no doubt plays an important role given the microstructures of these materials. This justifies the assumption of negligible radiation within the anode and cathode layers, which is made in the majority of previous SOFC heat transfer studies [1–3,6].

It should be noted that there is some question of how accurately the radiative properties of the bulk electrode and electrolyte materials describe those of the corresponding layers within an SOFC. The scattering behaviour of the YSZ electrolyte is particularly questionable, given that the pore spacing is approximately the same order of magnitude as the electrolyte layer thickness. Furthermore, the porosity values of SOFC electrolytes typically range between 0 and 5%, so 6% is a somewhat high value.

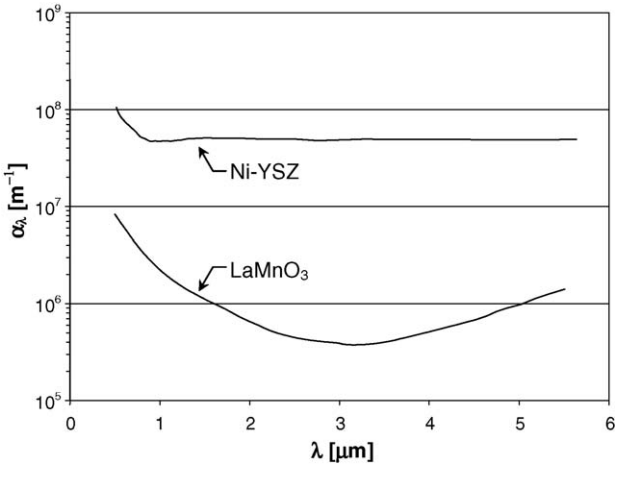

Fig. 4. Absorption coefficients for bulk anode and cathode materials.

4. Heat transfer model

4.1. Computational domain

Due to the complex nature of SOFCs (which involve multicomponent flow, multimode heat transfer, and electrochemistry) and the size of the computational domain, detailed CFD simulations are notoriously expensive and can incorporate only the simplest radiation models while still remaining computationally tractable. Because of this, our analysis is instead based on a 2-D conduction/radiation problem with heat transfer characteristics similar to a SOFC, but is simple enough to accommodate more detailed radiation models that can accurately assess the importance of thermal radiation in the electrode/electrolyte layers.

This model is based on a 0.1 m long counter-flow anode-supported SOFC geometry shown in Fig. 5(a). The fuel and air channels are 1 mm wide, and the anode, electrolyte, and cathode layer thicknesses are 500, 15, and 50 μm, respectively. The thermal conductivities of the electrodes and electrolyte are given in Table 1, and the composition and properties of the fuel and air are summarized in Table 2. The radiation sub-domain, shown in Fig. 5(b) includes only the electrolyte layer, due to the aforementioned opacity of the electrodes.

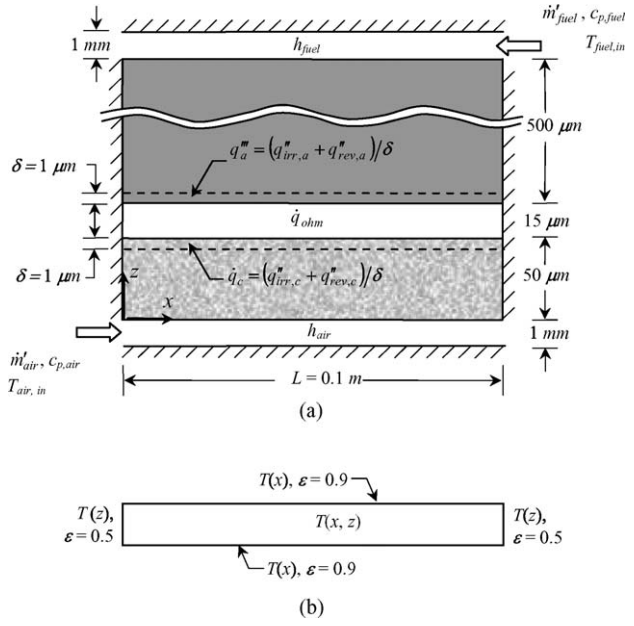

Fig. 5. Heat transfer model: (a) conduction domain, (b) radiation domain.

4.2. Boundary conditions

Four boundary conditions must be prescribed over the edges of the computational domain in order to solve for the temperature field.

A convection boundary condition is prescribed over the upper and lower surfaces of the anode and cathode layers, respectively. The air and fuel bulk inlet temperatures are set equal to 950 K and a uniform current density of 4000 A m^{-2} is assumed, typical values for this type of fuel cell. The air flow rate is calculated by modifying Eq. (1)

$$\dot{m}'_{\text{air}} = \frac{i''}{4Fu_{\text{O}_2}} L \frac{n_{\text{air}}}{n_{\text{O}_2}} M_{\text{air}}, \tag{9}$$

where L is the length of the air channel, u_{O_2} the oxygen utilization rate, M_{air} the molar mass of air, and $n_{\text{air}}/n_{\text{O}_2}$ the number of moles of air containing 1 mol of O_2. The mass flow rate of fuel is calculated based on Eq. (2) in a similar way

$$\dot{m}'_{\text{fuel}} = \frac{i''}{2Fu_{\text{H}_2}} L \frac{n_{\text{fuel}}}{n_{\text{H}_2}} M_{\text{fuel}}, \tag{10}$$

where u_{H_2} is the hydrogen utilization rate, M_{fuel} the molar mass of fuel, and $n_{\text{fuel}}/n_{\text{H}_2}$ the number of moles of fuel containing 1 mol of H_2. Substituting the properties in Table 2 into Eqs. (9) and (10) and assuming oxygen and hydrogen utilization rates of 20 and 80% respectively gives $\dot{m}'_{\text{air}} = 6.649 \times 10^{-4}$ kg ms^{-1}, and $\dot{m}'_{\text{fuel}} = 6.452 \times 10^{-4}$ kg ms^{-1}.

The convection coefficients in the air and fuel channels are found using the Nusselt number for laminar flow through a slot in which one surface is adiabatic and the other surface has a constant heat flux boundary condition, $Nu_{D_{\text{h}}} = 5.385$ [24], where the hydraulic diameter, D_{h} is equal to the channel half-width. Carrying out the calculations gives $h_{\text{air}} = 181$ W m^{-2} K^{-1} and $h_{\text{fuel}} = 215$ W m^{-2} K^{-1}.

Heat generation terms in the anode, cathode, and electrolyte are calculated as described in the previous section assuming a uniform current density of 4000 A m^{-2}, anodic and cathodic overpotentials of 1 V [11] and 1.5 V [12] respectively, and an electrolyte ionic resistivity $\rho_{\text{e}} = 0.8901\ \Omega$ m [13]. The corresponding heat generation terms are summarized in Table 3. Since it is impractical to prescribe a planar heat source between interior control volumes, heat generation at the electrode/electrolyte interfaces is assumed to occur uniformly within a reaction zone on the electrode side having a thickness of 1 μm as indicated in Fig. 5(a).

Table 2
Composition and properties of air and fuel

Property	Air	Fuel
ρ (kg m^{-3})	0.399	0.255
c_p (kJ kg^{-1} K^{-1})	1.129	1.673
k (W m^{-1} K^{-1})	0.067	0.080
y_{O_2}	0.225	0
y_{H_2}	0	0.85
y_{N_2}	0.775	0.10
$y_{\text{H}_2\text{O}}$	0	0.05

Table 3
Heat generation terms in SOFC layers

Layer	Source term
Anode	$q''_{\text{irr,a}} = 0.6$ kW m^{-2} $q''_{\text{rev,a}} = -0.6$ kW m^{-2}
Cathode	$q''_{\text{irr,c}} = 0.4$ kW m^{-2} $q''_{\text{rev,c}} = 1.7$ kW m^{-2}
Electrolyte	$q'''_{\text{ohm}} = 14.7 \times 10^3$ kW m^{-3}

The boundary conditions of the radiation sub-domain are specified with the temperature obtained from the most recent conduction solution. The emissivities of the upper and lower boundaries, representing the anode/electrolyte and cathode/electrolyte interfaces respectively, are assumed to be 0.9, which is reasonable for a porous ceramic surface. The emissivities of the lateral surfaces are set equal to 0.5, which is typical for a rough, lightly-oxidized metal surface. The porous medium is treated as grey and the absorption and scattering coefficients are set equal to the Planck mean values evaluated at 1000 K; this is a reasonable assumption, given the small degree of temperature variation over the radiation domain.

4.3. Solution technique

The solution procedure is initialized by solving the temperature field over the conduction domain using a second-order finite volume method coupled with a first-order upwind scheme in the fuel and air channels. This temperature field is projected onto the radiation domain and boundaries, which in turn is solved for the radiative source term within the electrolyte and radiative fluxes crossing the electrolyte boundaries. These terms are added to the energy equations and boundary conditions on the conduction domain, which is again solved for the temperature field. This process continues until convergence is obtained.

Two different radiation solvers are employed to solve for the radiation source term in the electrolyte: the Schuster–Schwarzschild two-flux method [25] and a collision-based Monte Carlo method [26]. The Schuster–Schwarzschild method assumes 1D radiation heat transfer, specifically that the intensity at any point within the medium is isotropic over a hemisphere centered in the direction of radiation heat transfer and is also isotropic over the complementary hemisphere. These assumptions transform the radiative transfer equation (RTE) into a coupled system of two first-order ordinary differential equations that can be easily solved over the problem domain using traditional numerical methods. The Schuster–Schwarzschild method is one of the oldest RTE solution techniques, and is still used to analyze systems in which radiation heat transfer is demonstrably 1D (e.g. thermal barrier coatings) and where other, more complex heat transfer modes dominate the problem, necessitating computational economy. Both Murthy and Fedorov [5] and Damm and Fedorov [6] used this method in their SOFC

analyses by assuming 1D radiation heat transfer between the electrodes.

The Monte Carlo method is more accurate than the Schuster–Schawrzchild method, but it is also more expensive. The first step of the analysis is to specify the energy of a single photon. A large number of photon bundles are then emitted in random directions from random locations over each volume and surface element, according to predefined probability density functions; the number of emitted bundles is proportional to the emissive energy of the element. Each time a photon bundle is emitted, the distance the bundle travels before it is either scattered or absorbed is calculated using a probability density function based on the total extinction coefficient. The bundle is then raytraced as it travels through volume elements and intercepts wall elements. Each time the bundle intercepts a wall element, it is either absorbed or diffusely-reflected depending upon the value of the wall emissivity relative to a randomly-generated number between zero and unity. If the bundle travels a distance equal to its pathlength without being absorbed by a wall element, it is either absorbed by the current volume element or scattered into a new direction based on the relative value of the scattering albedo, $\Omega = \sigma_s/(\sigma_s + \alpha)$, and a randomly-generated number between zero and unity. Once all bundles have been emitted and absorbed, the radiative source terms and heat fluxes are computed by subtracting the energy emitted by the volume and surface elements (the number of emitted bundles times the energy per bundle) from the energy absorbed throughout the process. Although it is one of the most accurate schemes for solving radiation heat transfer problems, the Monte Carlo method is too expensive to be incorporated into a full SOFC simulation, and is only used here to treat the simplified problem shown in Fig. 5.

5. Results and discussion

5.1. Validation

The radiation/conduction solvers are first validated by using them to solve the 1-D benchmark problem of Crosbie and Viskanta [27], who provide the conduction and radiation heat flux between two temperature-specified parallel grey walls that bound an absorbing, emitting, and scattering medium. The 1-D problem is approximated by a 2-D problem having an aspect ratio of 20:1 shown in Fig. 6, and the results are taken from the x-midplane. Table 4 shows that the total

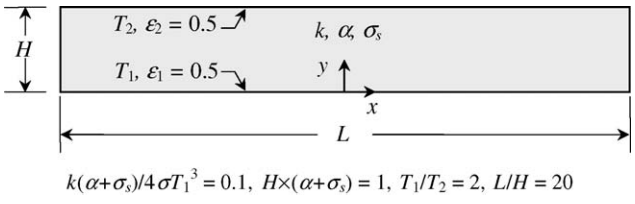

Fig. 6. Benchmark problem.

Table 4
Model and benchmark results

$\sigma_s/(\sigma_s+\alpha)$	$q_{12}/\sigma T_1^4$		
	Schuster–Schwarzchild	Monte Carlo	Benchmark solution [27]
0	0.546	0.558	0.571
0.5	0.502	0.518	0.513
1	0.434	0.447	0.449

(non-dimensional) heat flux across the two plates obtained using the Schuster–Schwarzchild and Monte Carlo methods for different scattering albedo values are within 5% of the benchmark solutions.

5.2. Influence of radiation on temperature distribution

Next, the importance of radiation heat transfer is assessed by comparing the temperature fields within the electrolyte layer found using the coupled conduction/radiation solvers to the one obtained using the conduction solver alone. The computational domain was split into a total of 6000 elements, with 1500 of these in the electrolyte. This level of refinement was verified to be sufficient for grid-independence by performing a refinement study on the conduction solution. The Schuster–Schwarzchild simulation used the same grid as the conduction solution while the Monte Carlo analysis was carried out by emitting approximately 3×10^9 bundles per iteration.

The temperature distributions along the horizontal and vertical electrolyte midplanes obtained by the three methods are shown in Figs. 7 and 8. In Fig. 7, the temperature distributions along the y-midplane obtained using the coupled Schuster–Schwarzchild/conduction and Monte Carlo/conduction solvers are indistinguishable from the conduction solution, which varies from 988 K at $x = 0$ to 1102 K at $x = 100$ mm, with a maximum temperature of 1346 K at $x = 71$ mm. Fig. 8 shows that upon closer inspection,

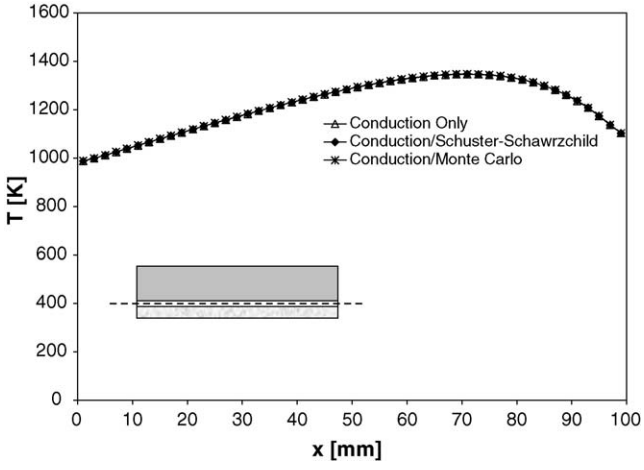

Fig. 7. Temperature distribution along z-midplane.

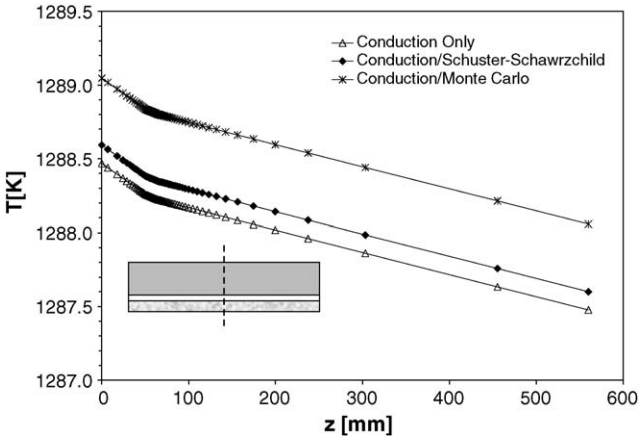

Fig. 8. Temperature distribution along x-midplane.

the temperature distributions along the x-midplane obtained using the Schuster–Schwarzchild/conduction and Monte Carlo/conduction solvers are within 0.1 and 0.6 K of the conduction solution, respectively. The temperature profile obtained by the Monte Carlo method is likely higher than the Schuster–Schwarzchild solution because the former accommodates radiation heat transfer in the z-direction while the latter does not. Despite this, these differences are much smaller than the expected accuracy of the numerical simulation, suggesting that radiation within the electrolyte can be excluded from a heat transfer model without significant error.

This conclusion was also reached by Damm and Fedorov [6], but not by Murthy and Fedorov [5]; the former found that neglecting radiation results in errors of less than 1 K in the temperature field of an anode-supported SOFC, while the latter claims that this assumption leads to errors larger than 100 K within an electrolyte-supported SOFC. Damm and Fedorov [6] account for this difference by noting that the temperature variation between the electrodes in an electrolyte-supported SOFC is much larger than that of an electrode-supported SOFC due to the comparatively high conduction resistance across the electrolyte in the former type of fuel cell. As shown in Table 5, Murthy and Fedorov [5] also assumed a smaller electrolyte extinction coefficient compared to values used by Damm and Fedorov [6] and the present work, which are more in line with extinction coefficients cited in other experimental and theoretical studies. This is, in fact, more likely to be the reason why the conclusions made by these papers are different.

Table 5
Electrolyte radiative properties

	$\sigma_s + \alpha$ (m^{-1})	$\Omega = \sigma_s/(\sigma_s + \alpha)$
Murthy and Fedorov [5]	500	0
Damm and Fedorov[a] [6]	1.02×10^4	0
Present study	1.03×10^4	0.97

[a] Planck mean value at 1000 K from three-band model.

Table 6
Maximum temperature difference between conduction and conduction/Monte Carlo solutions in the electrolyte

Configuration	Ω	Max ($\lvert T_{cond} - T_{cond/MC} \rvert$) (K)
Anode supported ($t_a = 500$ μm, $t_c = 50$ μm, $t_e = 15$ μm)	0.97	0.21
	0	0.17
Cathode supported ($t_a = 50$ μm, $t_c = 500$ μm, $t_e = 15$ μm)	0.97	0.47
	0	0.48
Electrolyte supported ($t_a = 50$ μm, $t_c = 50$ μm, $t_e = 150$ μm)	0.97	1.32
	0	2.22

In order to confirm this hypothesis, we also examined the effect of radiation heat transfer on the temperature fields of cathode- and electrolyte-supported SOFCs. Due to the aforementioned uncertainty of the electrolyte scattering coefficient we also modeled purely-absorbing electrolytes for the three configurations. These results are summarized in Table 6 as the maximum difference between the electrolyte temperature fields calculated using only the conduction solver and those obtained using the coupled conduction/Monte Carlo solver. These results show that radiation does indeed have a larger effect on the temperature field in the electrolyte-supported case compared to the electrode-supported cases, supporting the hypothesis of Damm and Fedorov [6] that radiation becomes more important as the conduction resistance between the electrodes increases. Nevertheless, the observed temperature differences for all configurations are less than 2 K, which again is small relative to the accuracy of the numerical simulation.

6. Conclusions

This paper evaluated the importance of thermal radiation heat transfer in the electrode and electrolyte layers within planar SOFCs. This was done by first characterizing the thermophysical and radiation properties of the component materials and then developing a 2D model of an anode-supported SOFC based on the sources of heat generation within the electrode and electrolyte layers. The importance and nature of thermal radiation was then determined by comparing the temperature distributions obtained using coupled Schuster–Schwarzchild/conduction and Monte Carlo/conduction solvers to the one calculated assuming conduction as the only mode of heat transfer.

The results show that thermal radiation has a negligible effect on the temperature field in the electrode and electrolyte layers. Due to the minor effect thermal radiation has on the temperature field (which is likely smaller in magnitude than errors induced by modeling assumptions) thermal radiation can safely be excluded from a detailed CFD analysis of a planar anode-supported SOFC.

Acknowledgement

The authors would like to thank Drs. Gisele Amow, Serguei Koutcheiko, Daniel Poitras, and Xinge Zhang for their helpful discussions regarding the thermophysical and optical properties of SOFC materials and Mr. Ron Jerome for computer support.

References

[1] H. Yakabe, T. Ogiwara, M. Hishinuma, I. Yasuda, J. Power Sources 102 (2001) 144–154.
[2] J.D.J. VanderSteen, J.G. Pharaoh, Proceedings of the ICHMT Fourth International Symposium on Radiative Transfer, Istanbul, Turkey, June 20–25, 2004.
[3] J.D.J. VanderSteen, M.E. Austin, J.G. Pharoah, Proceedings of the ASME Second International Conference on Fuel Cell Science Engineering and Technology, Rochester, NY, June 14–16, 2004.
[4] R. Siegel, ASME J. Heat Transf. 121 (1999) 478–481.
[5] S. Murthy, A.G. Fedorov, J. Power Sources 124 (2003) 453–458.
[6] D.L. Damm, A.G. Fedorov, Proceedings of the ASME IMECE, Anaheim, CA, November 13–19, 2004.
[7] S.B. Beale, Solid oxide fuel cell, in: B. Sundén, M. Faghri (Eds.), Transport phenomena in Fuel Cells, WIT Press, Southampton, UK, 2005.
[8] S.B. Beale, Y. Lin, Proceedings of the Third International Conference on Computational Fluid Dynamics in the Minerals and Process Industries, Melbourne, Australia, 2003.
[9] M.A. Khaleel, J.R. Selman, in: S. Singhal, K. Kendall (Eds.), High Temperature Solid Oxide Fuel Cells, Elsevier, London, UK, 2003, pp. 291–331.
[10] K. Kanamura, S. Yoshioka, Z. Takehara, J. Electrochem. Soc. 138 (1991) 2165–2167.
[11] W. Huebner, H.U. Anderson, Proceedings of the FETC Fuel Cell Review Meeting, Morgantown, WV, August 20–21, 1996.
[12] W. Huebner, H.U. Anderson, Proceedings of the FETC Fuel Cell Review Meeting, Morgantown, WV, August 26–28, 1997.
[13] P. Costamagna, K. Honegger, J. Electrochem. Soc. 145 (1998) 3995–4006.
[14] K.W. Schlicting, N.P. Padture, P.G. Klemens, J. Mater. Sci. 36 (2001) 3003–3010.
[15] T. Nishikawa, D. Ogawa, S. Honda, H. Awaji, J. Soc. Mater. Sci. Jpn. 52 (2003) 581–591.
[16] T. Kawashima, M. Hishinuma, JIM Mater. Trans. 37 (1996) 1518–1524.
[17] T. Makino, T. Kunitomo, I. Sakai, H. Kinoshita, Heat Transf.: Jpn. Res. 13 (1985) 33–50.
[18] H.C. Van de Hulst, Light Scattering by Small Particles, Wiley, New York, NY, 1957, pp. 172–179.
[19] D.L. Wood, K. Nassau, Appl. Opt. 21 (1982) 2978–2981.
[20] M.F. Modest, Radiative Heat Transfer, McGraw-Hill, New York, NY, 1993, 444 pp.
[21] Y. Okimoto, T. Katsufuji, T. Ishikawa, A. Urushibara, T. Arima, Y. Tokura, Phys. Rev. Lett. 75 (1995) 109–112.
[22] G.A. Niklasson, C.G. Granqvist, J. Appl. Phys. 55 (1984) 3382–3410.
[23] E.D. Palik, Handbook of Optical Constants, Academic Press, San Diego, CA, 1985, 317 pp.
[24] R.K. Shah, A.L. London, Laminar Flow Forced Convection in Ducts: A Source Book for Compact Heat Exchanger Analytical Data, Academic Press, New York, NY, 1978, 157 pp.
[25] R. Siegel, J.R. Howell, Thermal Radiation Heat Transfer, 4th ed., Taylor & Francis, New York, NY, 2002, pp. 681–682.
[26] J.T. Farmer, J.R. Howell, in: J.P. Hartnett, et al. (Eds.), Advances in Heat Transfer, vol. 31, Academic Press, San Diego, CA, 1998, pp. 333–429.
[27] A.L. Crosbie, R. Viskanta, Waérme Stoffuebertrag 4 (1971) 205–212.